Pergamon

Int. J. Multiphase Flow Vol. 22, No. 2, pp. 335–352, 1996

0301-9322(95)00068-2
0301-9322/96 $15.00 + 0.00

DIRECT SIMULATION OF FLOWS OF SOLID–LIQUID MIXTURES

H. H. HU

Department of Mechanical Engineering and Applied Mechanics, University of Pennyslvania, Philadelphia, PA 19104-6315, U.S.A.

(Received 15 August 1995; in revised form 9 September 1995)

Abstract—A finite element technique based on moving unstructured grids is developed to simulate the motion of a large number of solid particles in a flowing liquid. A generalized Galerkin finite element formulation which incorporates both the fluid and particle equations of motion into a single variational equation is developed for Newtonian fluids. The hydrodynamic forces and moments acting on the solid particles are eliminated in the formulation, so need not be computed explicitly. An arbitrary Lagrangian–Eulerian (ALE) technique is adopted to deal with the motion of the particles. In the implementation, the nodes on the particle surface are assumed to move with the particle. The nodes in the interior of the fluid are computed using Laplace's equation, to guarantee a smoothly varying distribution of the nodes. At each time step, the grid is updated according to the motion of the particles and checked for element degeneration. If unacceptable element distortion is detected, a new finite element grid is generated and the flow fields are projected from the old grid to the new grid. This generalized ALE Galerkin finite element approach gives rise to a set of non-linear algebraic equations which is solved via a quasi-Newton scheme. The corresponding linearized system is solved with an iterative solver using a preconditioned generalized minimal residual algorithm. Initially, the particles are positioned randomly in the fluid, with zero velocity. The particles are then released and the motion of the combined fluid–particle system is simulated using a procedure in which the positions of the particles and of the mesh grids are updated explicitly, while the velocities of the fluid and the solid particles are determined implicitly.

Using the developed numerical procedure, we study the Poiseuille flow of solid–liquid mixtures in a vertical channel. The computation is performed within a unit cell which is periodic in the direction along the channel. The gravity is directed along the channel walls, and a pressure gradient is applied against the gravity and drives the flow. The solid particles are slightly heavier than the liquid. The effects of the applied pressure gradient, the particle Reynolds number and the fraction of the solid loading on the flow pattern of the solid–liquid mixture are studied. It was found that when the applied pressure gradient is large enough to overcome the gravity, the particles migrate away from the channel walls and there is a clear liquid layer next to the wall which lubricates the flow. As the particle Reynolds number is increased, particles interact more strongly and large clusters of particles are formed in the flow.

1. INTRODUCTION

Solid–liquid two-phase flows are usually studied using a continuum approach that views solids and liquids as inter-penetrating mixtures, each being governed by conservation laws, either postulated or derived by averaging [see Ishii (1975), Drew (1983), Joseph & Lundgren (1990) and Zhang & Prosperetti (1994), for example]. This approach results in unknown terms representing interactions between the liquid and solid phases. These terms must be modeled to close the equations (Anderson & Jackson 1967). The nature of the detailed interactions between solids and liquids cannot be understood from the application of the mixture theories.

The clusters and anisotropic microstructures observed in solid–liquid flows are the result of solid particle migrations produced by particle–particle and particle–wall interactions. These local rearrangement mechanisms are mediated by things like hydrodynamic forces and moments acting on the particles, wake interactions and vortex shedding. Direct numerical simulation of the exact particle motion in liquid may be the only theoretical tool capable of studying these non-linear and geometrically complicated phenomena.

It is possible to simplify the flow description considerably by ignoring viscous effects completely (inviscid potential flow) or by ignoring inertia completely (Stokes flow). Potential flow simulations [see, Sangani & Didwania (1993), Sangani & Prosperetti (1993) and Smereka (1993)] do lead to

cross-stream alignment of particles in fluidized systems, but the wakes and the other non-linear mechanisms for the fundamental arrangement of particles in a fluidized suspension are absent. Brady and coworkers [see, for example, Brady & Bossis (1988) and Brady (1993)] have developed numerical techniques for simulating the motion of a large number of particles in Stokes flow. These simulations are appropriate for colloids in the limit of very small Reynolds numbers and appear to successfully capture the hydrodynamic interactions of the particles. However, the non-linear inertia mechanisms which control the migration and the rotation of particles do not exist in Stokes flow.

For simulations of solid–liquid flows at finite Reynolds numbers, Hu *et al.* (1992) developd a numerical scheme using a finite element technique and simulated two-dimensional motions of a few (up to four) sedimenting circular and elliptic cylinders confined in a channel. Using the same scheme, Feng *et al.* (1994a, b) studied the motion and interaction of circular and elliptical particles in sedimenting, Couette and Poiseuille flows of a Newtonian fluid. Huang *et al.* (1994) examined the turning couples on an elliptic particles settling in a channel. Hu (1996) studied the rotation of a circular cylinder setting close to a solid wall. Feng *et al.* (1995) analysed the mechanisms for the lifting of flying capsules in pipelines. A summary of these numerical works was presented by Joseph (1994).

Based on a space–time finite element method advocated by Hughes [see Hughes *et al.* (1987) and Huges & Hulbert (1988)], Tezduyar *et al.* (1992a, b) developed a DSD/ST (deforming-spatial-domain/space–time) procedure for finite element computations involving moving boundaries and interfaces. In their method, the finite element solution and test functions extend over both the spatial and temporal coordinates. The basis functions are continuous in space but discontinuous in time with a jump term in the variational formulation enforcing the weak continuity of solution across space–time slabs. They tested their method for flows with drafting cylinders. Using the same stabilized space–time finite element method, Johnson & Tezduyar (1995) recently simulated sedimentation of up to five solid spheres in a tube at a Reynolds number of 100. They developed an automatic mesh updating technique based on solving an equation governing the motion of the mesh nodes and on remeshing to accommodate the change in the shape of the domain.

In the references mentioned above, only a few particles are involved. Unverdi & Tryggvason (1992) introduced a front tracking/finite difference method for computing the unsteady motion of drops and bubbles. In their work, the flow field is solved on a fixed uniform grid using the finite difference scheme. The drop surface is tracked by a set of points (front) that are moved by interpolating their velocity from the fixed grid. In the discretization, the sharp drop surface is replaced by a smoother grid interface. However, the front points are reconstructed to keep the density and viscosity stratification sharp and to calculate surface tension forces at each time step. Esmaeeli & Tryggvason (1995) have computed the rise of 16 bubbles in three dimensions, and 144 and 324 two-dimensional bubbles in a doubly periodic domain at a Reynolds number near 2. These simulations have not been adapted to flows with solid particles.

A new unconventional computational approach to the solid–liquid flow is based on the lattice–gas [see, for example, Ladd *et al.* (1988)] and lattice Boltzmann methods (Ladd, 1994). These models can handle a huge number of particles. However, the conditions used in these methods are not directly comparable to the experimental ones, and the results produced by these methods are not sufficiently reliable to be used in engineering practices.

In this paper, we will present a finite element technique based on moving unstructured grids to simulate motion of a large number of solid particles in a flow liquid.

2. GOVERNING EQUATIONS

Consider an incompressible fluid occupying a bounded region Ω_t with boundary Γ_t at a given time instant t. There are N rigid solid objects (particles) freely moving in the fluid. We are interested in determining the motion of both fluid and individual solid particles. The Reynolds number of the flow based on particle size is not small, thus the inertia of the fluid and solid cannot be neglected. The fluid motion has to satisfy the conservation of mass

$$\nabla \cdot \mathbf{u} = 0 \qquad [1]$$

and the conservation of momentum

$$\rho_f\left(\frac{\partial \mathbf{u}}{\partial t} + (\mathbf{u}\cdot\nabla)\mathbf{u}\right) = \rho_f \mathbf{f} + \nabla\cdot\sigma \tag{2}$$

where $\mathbf{u}$ is the velocity vector, ρ_f is the density of the fluid, $\mathbf{f}$ is the body force and σ is the stress tensor. For a Newtonian fluid the stress tensor is given by the simple constitutive relation

$$\sigma = -p\mathbf{1} + \mu_f[\nabla\mathbf{u} + (\nabla\mathbf{u})^T] \tag{3}$$

where p is the pressure and μ_f is the viscosity of the fluid.

The motion of solid objects satisfies Newton's law

$$\mathbf{M}\frac{d\mathbf{U}_p}{dt} = \mathbf{F}_p + \mathbf{G}_p \tag{4a}$$

and

$$\frac{d\mathbf{X}}{dt} = \mathbf{U}_p, \quad \text{for} \quad p = 1, 2, \ldots, N \tag{4b}$$

where $\mathbf{M}$ is the genrealized mass matrix. $\mathbf{X}$ and $\mathbf{U}$ are, respectively, the generalized position and velocity vectors which incorporate both translational and angular components. The generalized force vector is expressed in two terms: $\mathbf{F}$ is the force imposed on the particle by the fluid and $\mathbf{G}$ is the body force exerted by external fields such as gravity. The matrix and vectors are written explicitly as

$$\mathbf{M} = \begin{bmatrix} m & 0 & 0 & 0 & 0 & 0 \\ 0 & m & 0 & 0 & 0 & 0 \\ 0 & 0 & m & 0 & 0 & 0 \\ 0 & 0 & 0 & I_{xx} & I_{xy} & I_{xz} \\ 0 & 0 & 0 & I_{yx} & I_{yy} & I_{yz} \\ 0 & 0 & 0 & I_{zx} & I_{zy} & I_{zz} \end{bmatrix}, \quad \mathbf{X} = \begin{bmatrix} X \\ Y \\ Z \\ \Theta_x \\ \Theta_y \\ \Theta_z \end{bmatrix}, \quad \mathbf{U} = \begin{bmatrix} V_x \\ V_y \\ V_z \\ \Omega_x \\ \Omega_y \\ \Omega_z \end{bmatrix}, \quad \mathbf{F} = \begin{bmatrix} F_x \\ F_y \\ F_z \\ T_x \\ T_y \\ T_z \end{bmatrix} \tag{5}$$

where m is the mass of the object, and Is are the moments of inertia and products of inertia of the object. For two-dimensional motions, the mass matrix reduces to diagonal $\mathbf{M} = \text{diag}(m, m, I_{zz})$.

The forces and moments imposed on an object by the fluid are given by

$$[F_x, F_y, F_z] = \int \sigma\cdot\hat{\mathbf{n}}\, d\Gamma \tag{6a}$$

and

$$[T_x, T_y, T_z] = \int (\mathbf{x} - \bar{\mathbf{X}}_p)\times(\sigma\cdot\hat{\mathbf{n}})\, d\Gamma \tag{6b}$$

where the integration is performed over the surface of the object, $\hat{\mathbf{n}}$ is the unit normal vector on the surface of the object pointing outward and $\bar{\mathbf{X}}_p = [X, Y, Z]^T$ is the position of the centroid of the object.

The boundary of the domain occupied by the fluid, Γ_t, can be decomposed into three non-overlapping section: $(\Gamma_t)_u$, $(\Gamma_t)_\sigma$ and $\bigcup_p (\Gamma_t)_p$, where $(\Gamma_t)_p$ is the surface of solid particle p. On these boundary sections the following types of boundary conditions are imposed

$$\mathbf{u} = \mathbf{g}, \quad \text{on } (\Gamma_t)_u \tag{7}$$

$$\sigma\cdot\mathbf{n} = \mathbf{h}, \quad \text{on } (\Gamma_t)_\sigma \tag{8}$$

and

$$\mathbf{u} = \mathbf{V}_p + \boldsymbol{\Omega}_p\times(\mathbf{x} - \bar{\mathbf{X}}_p), \quad \text{on } (\Gamma_t)_p, \quad p = 1, 2, \ldots, N \tag{9}$$

where $\mathbf{g}$ and $\mathbf{h}$ are prescribed values of velocity and traction, $\mathbf{n}$ is the unit normal vector on the boundary and $\mathbf{V}_p$ and Ω_p are, respectively, the transitional and angular velocities of object p ($\mathbf{U}_p = [\mathbf{V}_p, \Omega_p]^T$). Equation [9] represents the no-slip condition on the surface of the object.

3. GALERKIN FINITE ELEMENT FORMULATION

We seek a generalized Galerkin finite element formulation that incorporates both the fluid and particle equations of motion [2] and [4]. In the formulation, the spatial coordinates are discretized using finite element scheme, and the temporal coordinate is treated with a finite difference method.

At time instant t, the fluid occupies the domain Ω_t with boundary Γ_t. We define the finite element interpolation functional space for the velocity and the pressure in the fluid phase as

$$S_{\mathbf{u}}^h = \{\mathbf{u}^h = (u_x^h, u_y^h, u_z^h) \,|\, \mathbf{u}^h \in H^{1h}(\Omega_t), \mathbf{u}^h = \mathbf{g}^h \text{ on } (\Gamma_t)_u,$$

and [10a]

$$\mathbf{u}^h = \mathbf{V}_p + \Omega_p \times (\mathbf{x} - \bar{\mathbf{X}}_p) \text{ on } (\Gamma_t)_p, \forall p = 1, \ldots, N\},$$

$$V_{\mathbf{w}}^h = \{\mathbf{w}^h = (w_x^h, w_y^h, w_z^h) | \mathbf{w}^h \in H^{1h}(\Omega_t), \mathbf{w}^h = 0 \text{ on } (\Gamma_t)_u,$$

and [10b]

$$\mathbf{w}^h = \delta\mathbf{V}_p + \delta\Omega_p \times (\mathbf{x} - \bar{\mathbf{X}}_p) \text{ on } (\Gamma_t)_p, \forall p = 1, \ldots, N\}$$

and

$$S_p^h = V_p^h = \{p^h | p^h \in H^{1h}(\Omega_t)\} \quad [10c]$$

where $\mathbf{V}_p$ and Ω_p ($\mathbf{U}_p = [\mathbf{V}_p, \Omega_p]^T$) are the translational and angular velocities of the solid particles, and $\delta\mathbf{V}_p$ and $\delta\Omega_p$ ($\delta\mathbf{U}_p = [\delta\mathbf{V}_p, \delta\Omega_p]^T$) are their variations (arbitrary functions of time). In the finite element domain, these spaces are formed using second-order polynomials for the velocity and first-order polynomials for the pressure (P_2/P_1 elements).

The Galerkin finite element formulation can be expressed as:

Find $\mathbf{u}^h \in S_{\mathbf{u}}^h$ and $p^h \in S_p^h$, such that $\forall \mathbf{w}^h \in V_{\mathbf{w}}^h$ and $q^h \in V_p^h$,

$$\int_{\Omega_t} \mathbf{w}^h \cdot \rho_f \left(\frac{\partial \mathbf{u}^h}{\partial t} + (\mathbf{u}^h \cdot \nabla)\mathbf{u}^h - \mathbf{f} \right) d\Omega + \int_{\Omega_t} \nabla \mathbf{w}^h : \sigma^h \, d\Omega - \int_{(\Gamma_t)_\sigma} \mathbf{w}^h \cdot \mathbf{h}^h \, d\Gamma$$

$$\underline{-\sum_p \int_{(\Gamma_t)_p} \mathbf{w}^h \cdot (\sigma^h \cdot \mathbf{n}) \Gamma} + \int_{\Omega_t} q^h \nabla \cdot \mathbf{u}^h \, d\Omega + \sum_p \delta\mathbf{U}_p \cdot \left(\mathbf{M} \frac{d\mathbf{U}_p}{dt} - \underline{\mathbf{F}_p} - \mathbf{G}_p \right) = 0. \quad [11]$$

Using the relation between $\mathbf{w}^h$ and $\delta\mathbf{U}_p$ on the surface of solid particles (built in $V_{\mathbf{w}}^h$) and [6] for the forces and moments acting on the particles, it can be easily shown that the integral over the particle surfaces cancels the generalized force term $\mathbf{F}_p$ (the two underlined terms). Therefore, in this generalized Galerkin formulation one does not need to compute explicitly the hydrodynamic forces and moments acting on the solid particles. A similar variational formulation was also developed by Hesla *et al.* (1995). An equivalent discretized form of [11] was used by Nomura & Hughes (1992) for study of fluid–structure interaction problems.

As we are expecting a large number of solid particles moving freely in the fluid, the domain occupied by fluid changes greatly. A moving finite element mesh has to be used. To handle the movement of the finite element mesh, an arbitrary Lagrangian–Eulerian (ALE) technique [see Huerta & Liu (1988) and Nomura & Hughes (1992)] is used. In this ALE Galerkin finite element formulation, [11] reduces to

$$\int_{\Omega_t} \mathbf{w}^h \cdot \rho_f \left[\frac{\delta \mathbf{u}^h}{\delta t} + (\mathbf{u}^h - \mathbf{u}_m^h) \cdot \nabla \mathbf{u}^h - \mathbf{f} \right] d\Omega + \int_{\Omega_t} \nabla \mathbf{w}^h : \sigma^h \, d\Omega - \int_{(\Gamma_t)_\sigma} \mathbf{w}^h \cdot d\Gamma$$

$$+ \int_{\Omega_t} q^h \nabla \cdot \mathbf{u}^h \, d\Omega + \sum_p \delta\mathbf{U}_p \cdot \left[\mathbf{M} \frac{d\mathbf{U}_p}{dt} - \mathbf{G}_p \right] = 0 \quad [12]$$

where $\delta \mathbf{u}^h/\delta t$ is the time derivative following the same referential mesh node and $\mathbf{u}_m^h$ is the velocity vector which defines the motion of mesh nodes. In general, the mesh velocity can be specified arbitrarily as long as it follows the motion of the particles. In our implementation, we assume that the nodes on the particles surface move with the particle (no slip), and the nodes in the interior of the fluid are computed using Laplace's equation, to guarantee a smoothly varying distribution of the nodes:

$$\nabla^2 \mathbf{u}_m = 0 \quad \text{in} \quad \Omega_t, \tag{13}$$

with boundary conditions given by

$$\mathbf{u}_m = \mathbf{u} = \mathbf{V}_p + \Omega_p \times (\mathbf{x} - \bar{\mathbf{X}}_p) \quad \text{on} \quad (\Gamma_t)_p, p = 1, 2, \ldots, N$$

and

$$\mathbf{u}_m = 0 \quad \text{on} \quad (\Gamma_t)_u \cup (\Gamma_t)_\sigma. \tag{14}$$

Equation [13] is also solved with a Galerkin finite element formulation whose functional space is formed using first-order (linear) polynomials, to reduce computational cost. The values of the mesh velocity on the remaining mesh nodes are interpolated locally inside each finite element.

The ALE finite element formulation [12] is related to the space–time finite element method with the basis functions continuous in space but discontinuous in time, as discussed in Hansbo (1992) and Behr & Tezduyar (1994). ALE formulation amounts to using elements that are superparametric in time. With a constant (P_0) temporal approximation of the solution, the geometry will be expressed by a linear (P_1) or quadratic (P_2) deforming element in space–time.

For a given finite element mesh, [12] can be discretized and be reduced to a non-linear system of algebraic equations

$$\begin{pmatrix} \mathbf{A} & \mathbf{B} & \mathbf{C} \\ \mathbf{B}^T & \mathbf{0} & \mathbf{0} \\ \mathbf{D} & \mathbf{E} & \mathbf{G} \end{pmatrix} \begin{pmatrix} \mathbf{u} \\ \mathbf{p} \\ \mathbf{U} \end{pmatrix} = \begin{pmatrix} \mathbf{a} \\ \mathbf{0} \\ \mathbf{b} \end{pmatrix}; \tag{15}$$

and [13] can be discretized to a linear system of algebraic equations

$$\mathbf{H}\mathbf{u}_m = \mathbf{c} \tag{16}$$

where **A**, **B**, **C**, **D**, **E**, **G** and **H** are sparse matrices. In general, **A** is non-symmetric and linear in **u** and $\mathbf{u}_m$; **G** and **H** are symmetric and positive definite. In [15] and [16], **u**, **p** and $\mathbf{u}_m$ represent, respectively, the vectors collecting all the velocity, pressure and mesh velocity unknowns at grid points in the fluid; and **U** is the vector combining all the translational and angular velocities of the solid particles. The vectors on the right hand side of the equations, **a**, **b** and **c** result from the force terms in the fluid and solid momentum equations and from the application of the boundary conditions. For two-dimensional flow problems, the length of the vector **u** is twice the number of nodes in the mesh; the length of **p** or $\mathbf{u}_m$ is the number of vertices in the mesh; and the length of the vector **U** is three times the number of rigid particles.

The algebraic systems [15] and [16] are coupled, and are solved iteratively at each time step. It is noted that the equations for the components of the mesh velocity are decoupled, and the matrix **H** in the algebraic systems [16] remains in the same form for a given finite element mesh. Thus, the matrix **H** is stored and repeatedly used during the iterations. It is also found that a modified version of [13], in which the Jacobian of the transformation between the physical and element domain is dropped, converges faster and also gives rise to better properties for the mesh velocity, when an iterative solver, such as GMRES, is used. In this modified version, smaller elements retain their shapes better, as noted by Johnson & Tezduyar (1994).

4. MESH GENERATION

Although the formulation of the problem described above is valid for general three-dimensional solid–liquid flows, we will concentrate on two-dimensional motions in the present study. We are anticipating rather complicated interactions of a large number of solid particles. The geometry of

the computation domain occupied by the fluid can change drastically from time to time. At each time step, the finite element mesh is updated according to the mesh velocity obtained at the previous time, and checked for element degeneration. If unacceptable element distortion is detected, a new finite element grid is generated which may not have any correspondence with the old grid, and then the flow field has to be projected from the old grid to the newly generated grid.

In computing solid–liquid flows with a large number of solid particles, it is often necessary to use periodic boundary conditions in one or more directions. At the periodic boundaries solid particles frequently leave and enter the computation domain. In this work we developed a finite element mesh generator that automatically takes care of the periodic boundaries without introducing artificial cuts on these boundaries. The artificial cuts on the periodic boundaries may give rise to very unsatisfactory elements. This mesh generator uses positions of the solid particles as input. The periodic boundaries are handled by developing proper mapping functions. In the case of two-dimensional flow within a unit cell which is periodic in one direction and bounded by solid walls in the other, the mapping is formed by first connecting two periodic boundaries resulting in a cylindrical surface, then expanding one end of the cylindrical surface to form a trapezoidal cone, and finally projecting the surface of the cone onto a two-dimensional concentric region. A preliminary mesh is generated inside this concentric region using the Delaunay–Voronoi methods [see for example, Hecht & Saltel (1990) and George (1991)]. This preliminary mesh is mapped back to the original periodic domain. The final mesh is obtained by performing a Delaunay triangulation and smoothing of the mapped mesh.

When a large number of solid particles interact, they may collide under certain conditions. In our current work, we assume that particles never collide and there is always a thin liquid film between the approaching particles. The mesh generator has a local refinement capability in the region (gaps) formed by approaching solid particles or between particles and bounding walls. There is always at least one layer of elements in those regions, and the mesh size in there is designed to be the minimum gap size between the approaching particles. The local refinement in the gaps between particles is essential to the correct modeling of the "particle collision" process.

An example of the mesh used in this study is presented in figure 1. There are 100 circular cylinders in a periodic domain between two channel walls. In the figure, straight line is used to connect three vertices of a triangle. However, the curved isoparametric P_2 triangles (with six nodes) are used in the simulation to fit the curved boundaries on the particle surface.

An additional cost incurred in using the unstructured finite element grid is the need to project flow field from one grid to another. In our projection scheme, for each node in the new mesh, a search is initiated in the old mesh to locate the element where the node lies. The search is essentially one-dimensional by using the information of neighboring elements. Once the element is identified, local coordinates for the node are calculated and various functions are easily interpolated.

5. SOLUTION PROCEDURE

Initially, the particles are positioned randomly in the fluid, with zero velocity. The fluid is either at rest or flowing steadily around the particles. The particles are then released, and the motion of the combined fluid–particle system is simulated. Hu *et al.* (1992) developed a solution procedure in which the positions of the particles and the grid nodes in the fluid domain are updated explicitly, while the particle velocities and the fluid flow field (velocity and pressure) are determined implicitly to avoid numerical instabilities. A modified version of that procedure which incorporates the ALE scheme with mesh velocities determined implicitly by solving a set of Laplace equations is implemented in this study. The details of the modified solution procedure are listed below.

(1) Initialization

$t_0 = 0$, $n = 0$ (index for time step).
Generate an initial mesh $\mathbf{x}_0$.
Initialize $\mathbf{u}(\mathbf{x}_0, 0)$, $p(\mathbf{x}_0, 0)$ and $\mathbf{X}_p(0)$, $\mathbf{U}_p(0)$ for $p = 1, 2, \ldots, N$.

(2) Explicit update

Select time step Δt_{n+1}: $t_{n+1} = t_n + \Delta t_{n+1}$.
Update particle position $\mathbf{X}_p(t_{n+1}) = \mathbf{X}_p(t_n) + \Delta t_{n+1}\mathbf{U}_p(t_n)$, for $p = 1, 2, \ldots, N$.
Update mesh nodes $\hat{\mathbf{x}}(t_{n+1}) = \mathbf{x}(t_n) + \Delta t_{n+1}\mathbf{u}_m(t_n)$.

(3) Remeshing and projection [if the mesh $\hat{\mathbf{x}}(t_{n+1})$ is too distorted]

Generate a new mesh $\mathbf{x}(t_{n+1})$.
Project the flow field from $\hat{\mathbf{x}}(t_{n+1})$ onto $\mathbf{x}(t_{n+1})$.

(4) Flow solver

Iteratively solve $\mathbf{u}(\mathbf{x}(t_{n+1}), t_{n+1}), p(\mathbf{x}(t_{n+1}), t_{n+1}), \mathbf{u}_m(\mathbf{x}(t_{n+1}), t_{n+1})$ and $\mathbf{U}_p(t_{n+1})$ for $p = 1, 2, \ldots, N$ from [15] and [16].

(5) If the time t_{n+1} is less than a specified time go to step (2); otherwise stop.

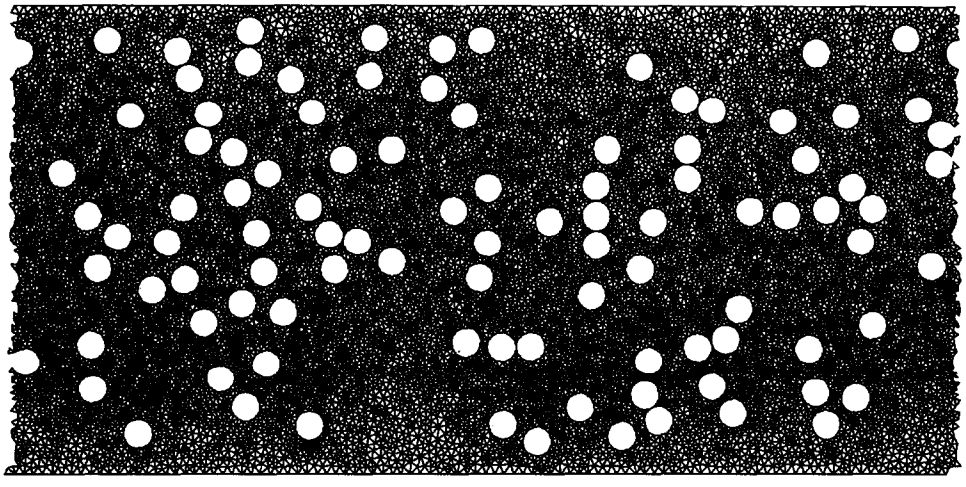

(a)

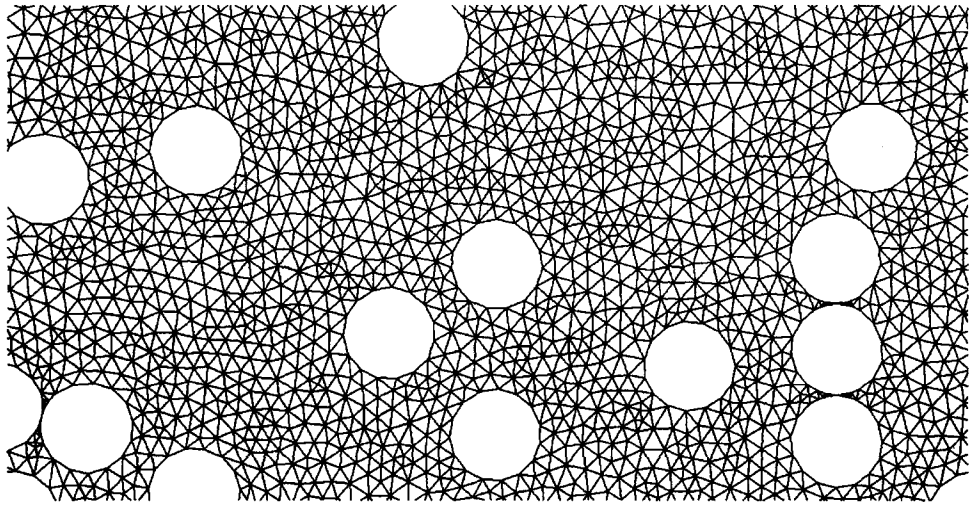

(b)

Figure 1. An example of the finite element mesh used in the simulation. (a) Overall view of a mesh with 100 circular cylinders. (b) Closer view at the center of the same mesh.

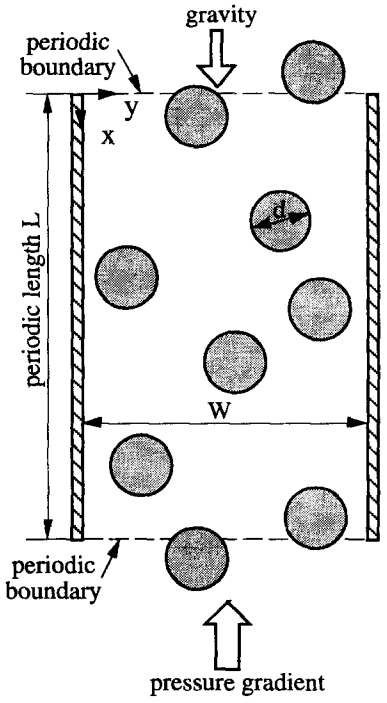

Figure 2. Sketch of the Poiseuille flow of a solid–liquid mixture.

In the procedure, the size of the time step Δt_{n+1} is determined by the maximum distance each particle is allowed to travel, or the maximum change in the particle speed. The explicit update step (2) is first-order accurate in time, which can be easily improved to second order by introducing accelerations of the solid particles and the mesh nodes. In the flow solver, the systems of algebraic equations [15] and [16] need to be solved iteratively. The non-linear system [15] is handled with a modified-Newton method, and treated as the outer iteration loop. The corresponding linearized algebraic system is solved with an iterative solver using a preconditioned generalized minimal residual (GMRES) procedure introduced by Saad & Schultz (1986). GMRES is a popular method for non-symmetric systems stemming from Navier–Stokes equations. In the GMRES procedure, the full system is projected onto a much smaller Krylov subspace, and the residual of the system is minimized on that subspace. To improve convergence of the iterations, the size of the Krylov space is set at 20 in this study. We also implemented a preconditioner using incomplete LU factorization with controlled threshold fill-in elements (ILUT). The number of fill-ins is controlled to be less than 10 for both the upper and lower triangular matrices. The implemented flow solver is quite robust and efficient.

6. RESULTS AND DISCUSSIONS

The program is tested against the numerical results computed using the code developed by Hu *et al.* (1992). For a sedimenting cylinder along the centerline of a channel, the computed terminal speed of the cylinder agrees with previously published numerical and theoretical results. The simulation of five sedimenting cylinders qualitatively reproduces drifting–kissing–tumbling.

In this paper, we present numerical results for Poiseuille flows of solid–liquid mixtures in a vertical channel. The flow geometry is sketched in figure 2. The solid particles are slightly heavier than the liquid. The gravity is directed along the channel walls and pointing in the positive x-direction. The pressure gradient is applied against the gravity and drives the flow. The width of the channel is W, and the periodic length of the computational cell is L. The particles in the fluid are circular and of uniform size with diameter d. The number of the particles, N, in the computational cell is specified and keeps fixed during the simulation.

The non-dimensional parameters governing the flow problem described above can be characterized as:

the relative channel width and length: $W/d, L/d,$ [17]

the solid fraction $\phi = \dfrac{N\pi d^2}{4LW},$ [18]

the density ratio $\rho_s/\rho_f,$ [19]

the particle Reynolds number $\mathrm{Re} = \rho_f V d/\mu_f,$ [20]

the driving pressure gradient $\mathrm{d}\bar{p} = \dfrac{-d}{\rho_f V^2}\left(\dfrac{\mathrm{d}p}{\mathrm{d}x} - \rho_f g\right)$ [21]

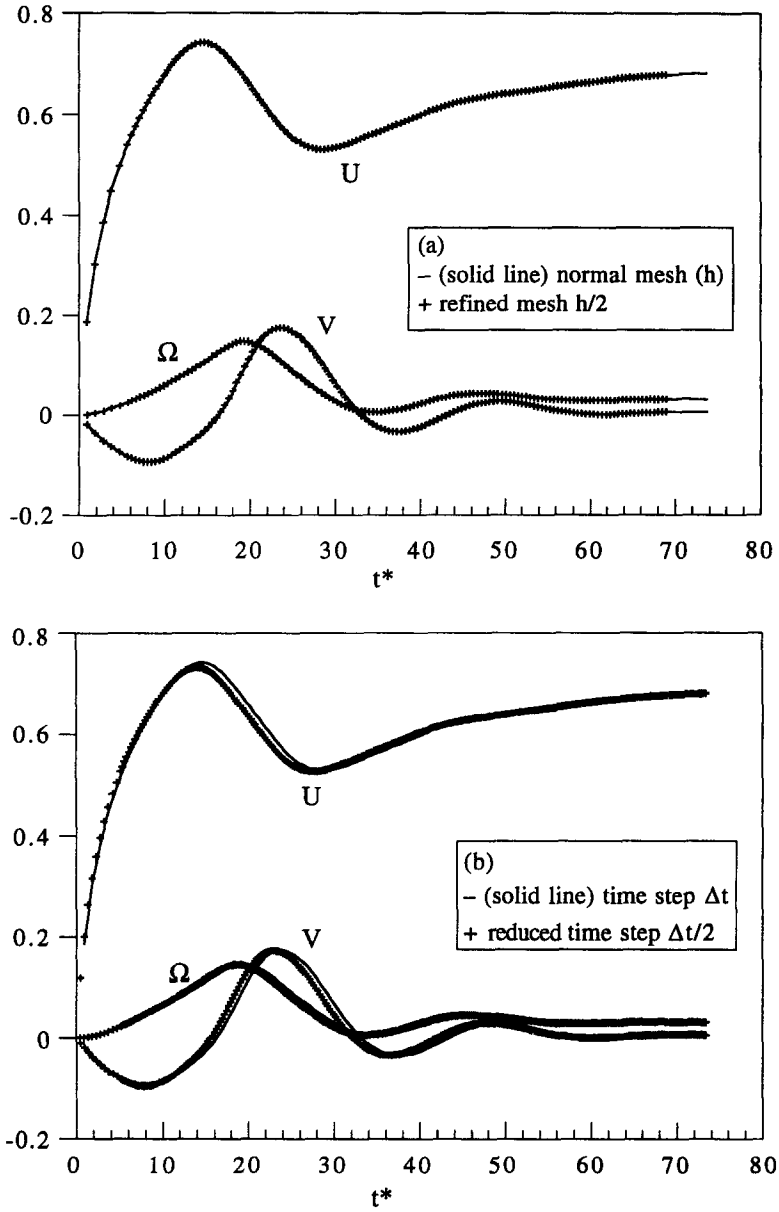

Figure 3. Convergence test with two particles ($N = 2$) at $W/d = 6$, $L/d = 8$, $\rho_s/\rho_f = 1.1$, $\mathrm{Re} = 9.44$ and $\mathrm{d}\bar{p} = 0.028$. The figures show the transients of the translational velocities U and V, and the angular velocity Ω of one of the cylinders. The dimensionless time t^* is defined as tV/d.

where V is the velocity scale for the flow, for example, to measure the difference in velocity between the solid particles and the fluid one can choose $V = \sqrt{(1 - \rho_f/\rho_s)gd}$. In defining the driving pressure gradient the static component is deducted and only the dynamic part is used. The solid–liquid mixture has a composite density

$$\rho_c = \rho_f + (\rho_s - \rho_f)\phi. \qquad [22]$$

To drive the mixture upward through the channel, the magnitude of the applied pressure gradient has to be greater than $\rho_c g$ which corresponds to a neutral non-dimensional pressure gradient $d\bar{p}_n = (\rho_s - \rho_f)g\phi d/\rho_f V^2$. In the simulation we control $d\bar{p}$ such that the flow could be upward $d\bar{p} > d\bar{p}_n$ (pressure driven) or downward $d\bar{p} < d\bar{p}_n$ (gravity driven).

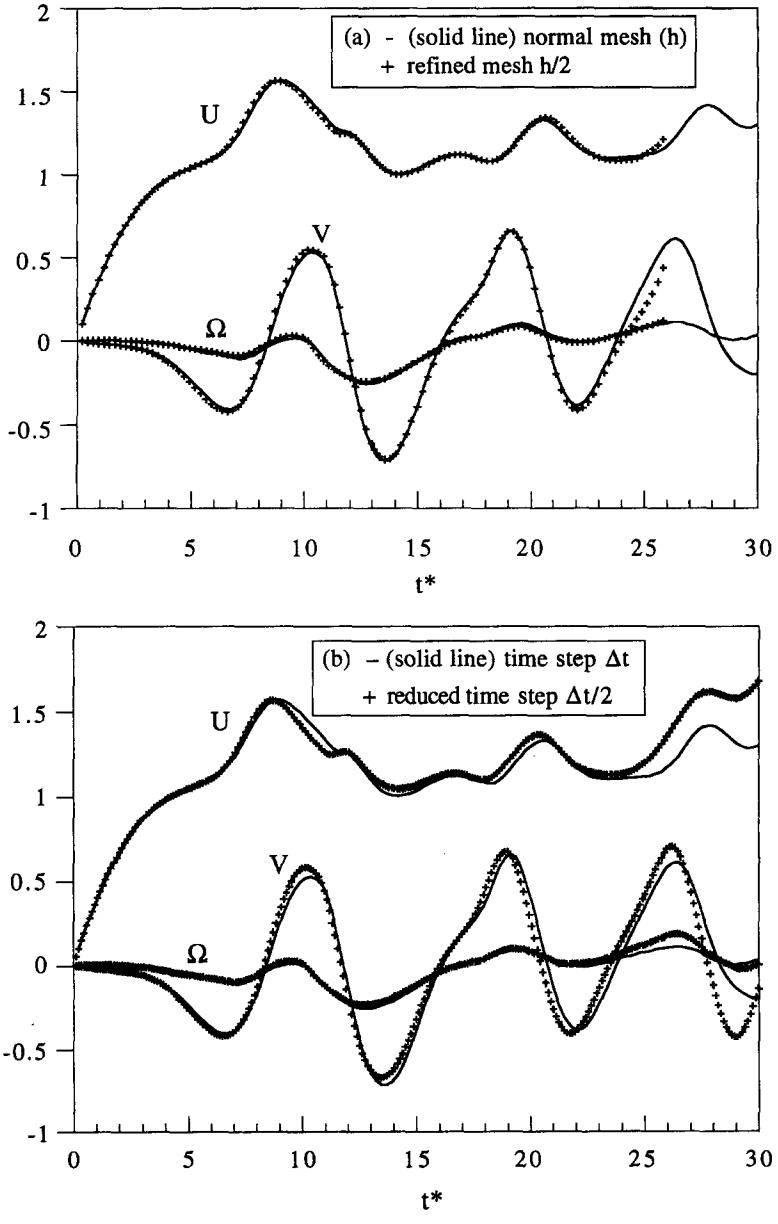

Figure 4. Convergence test with two particles ($N = 2$) at $W/d = 6$, $L/d = 8$, $\rho_s/\rho_f = 1.1$, Re = 94.4 and $d\bar{p} = 0.028$. The figures show the transients of the translational velocities U and V, and the angular velocity Ω of one of the cylinders.

The mesh size and time step to be used in the computation are determined by convergence tests. Two particles are used in the tests. The normal mesh size and time step are determined by the number of minimum segments ($=15$) on the particle surface, and by the maximum distance ($=0.4d$) each particle is allowed to travel, respectively. The mesh size and the time step are then reduced by half, the results are shown in figures 3 and 4 for particle Reynolds numbers of 9.44 and 94.4. For small Reynolds numbers, no noticeable differences were detected when a finer mesh or smaller time steps were used. For Re = 94.4, the mesh size and the time step used is still adequate. Only small differences wre detected at longer times. We think that those differences will not change the statistic information of the flow when a large umber of particles are involved.

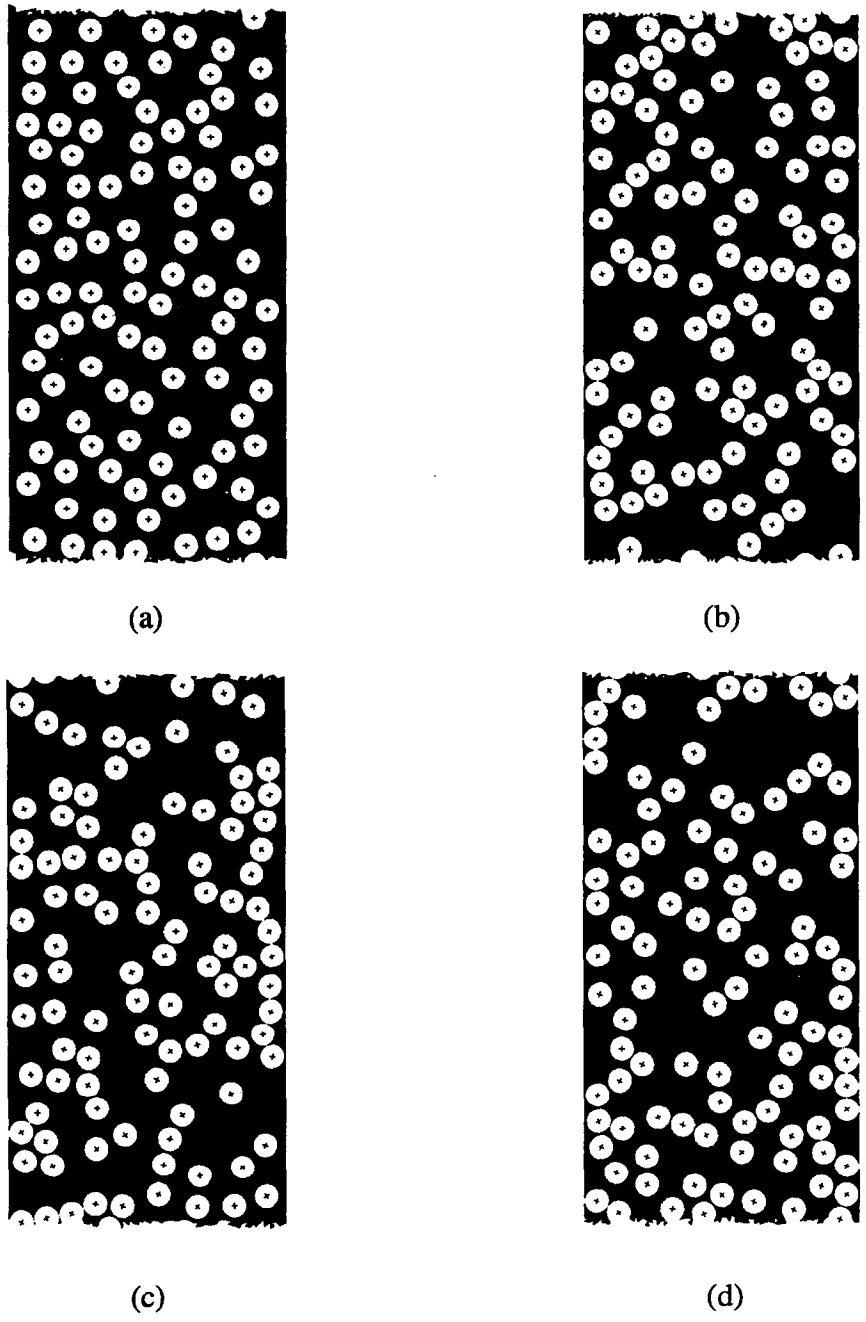

Figure 5. Down-flow with $W/d = 11$, $L/d = 22$, $\phi = 0.325$, $\rho_s/\rho_f = 1.1$, Re = 9.44, and $d\bar{p} = 0.336$. The figures show the snap shots of the flow field at four time instants (a) $t^* = 0$, (b) $t^* = 31.2$, (c) $t^* = 54.8$ and (d) $t^* = 98.0$, where t^* is the dimensionless time.

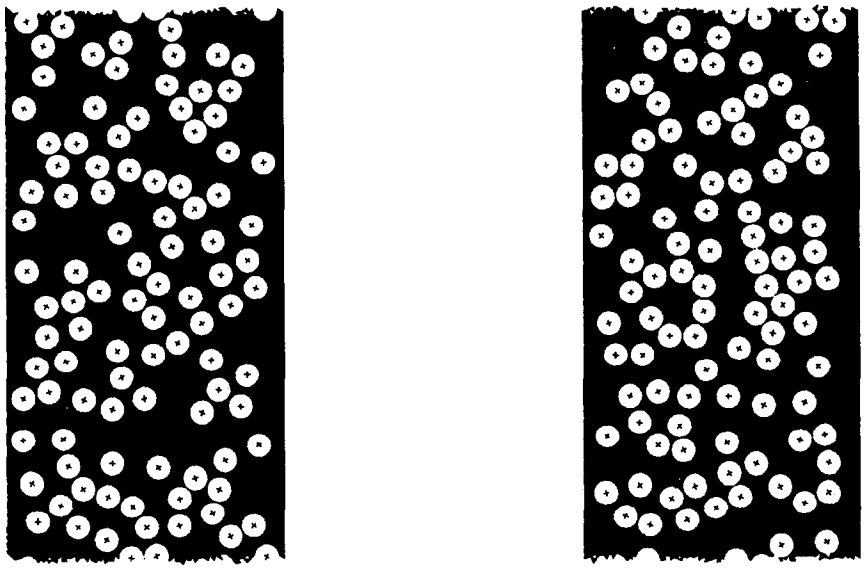

(a) (b)

Figure 6. Upflow with $W/d = 11$, $L/d = 22$, $\phi = 0.325$, $\rho_s/\rho_f = 1.1$, Re = 9.44 and $d\bar{p} = 0.449$. The figures show the snap shots of the flow field at two time instants, (a) $t^* = 24.7$ and (b) $t^* = 44.0$.

In the first simulation, the non-dimensional parameters are $W/d = 11$, $L/d = 22$, $\phi = 0.325$ ($N = 100$), $\rho_s/\rho_f = 1.1$, Re = 9.44 and $d\bar{p} = 0.336$ ($d\bar{p}_n = 0.358$). Particles in this flow are nearly neutrally suspended, since the applied pressure gradient almost balances the gravity. Figure 5 shows the flow field at four time instants. The white lines in the figure are stream lines. Initially the particles distribute randomly in the fluid as shown in figure 5(a). The particles are normally well separated from each other and from the channel walls. During the initial transient [figure 5(b)], the particles fall and the bulk of the fluid flows downward. During the sedimentation of the particles, long particle chains are formed along the streamlines, and they tumble due to the unstable nature of long bodies in Newtonian fluids. The particle–particle interaction can draw particles together and momentarily form particle clusters. As the flow field develops, the solid–fluid mixture at the middle of the channel starts to flow upwards, and circulation within the channel occurs, as indicated in figure 5(c). Eventually, an upflow stream is formed near the center of the channel, as shown in figure 5(d). The fluid and the particles near the walls flow slowly downward. Under this flow condition, particles tend to align along the walls, and stay there.

For the second simulation, we increase the applied pressure gradient $d\bar{p} = 0.449$ above the value for neutral suspension, and keep the other non-dimensional parameters the same. In this flow, the solid–liquid mixture flows upward. Figure 6 shows the flow field at two time instants. The initial distribution of the particles are the same as the previous simulation. After the initial transient, the mixture flows upward. The velocity profile in the channel is almost uniform, as evidenced by the even spacing of the iso-streamlines in figure 4(a) and (b). The most interesting feature for this flow is that the particles migrate away from the wall region and there is a clear liquid layer next to the channel walls where most of the shear occurs. This clear liquid layer forms a lubrication layer which facilitates the flow. The thickness of this lubrication layer is of the order of particle diameter. In this flow, the particles follow the fluid and do not interact as strongly as the previous case.

Next we examine the effect of the particle Reynolds number on the flow pattern. We increase the Reynolds number by a factor of 10 and keep the other parameters fixed. In the first case, the mixture flows downward. The non-dimensional parameters are $W/d = 11$, $L/d = 22$, $\phi = 0.325$, $\rho_s/\rho_f = 1.1$, Re = 94.4 and $d\bar{p} = 0.336$. The results are displayed in figure 7. The initial condition of the flow is the same as in figure 5(a). As the Reynolds number is increased, the particles interact

more strongly, and more structures (particle clusters and cross-stream arrays) are formed in the flow. Those particle clusters frequently break and reform. In this flow, there are no lubricating layers next the channel walls, instead the particles become close to each other (and may collide) and toward the channel walls, tend to stick to the walls. In the current version of the program, the collision process is not modeled, it is captured as far as the program can handle. If the size of the gap between the particles or the particle and the wall is less than 10^{-5} times the particle diameter, the simulation has to stop.

For the upward flow with the same high Reynolds number, the results are shown in figure 8. The particles are again interacting much more strongly than the lower Reynolds number case

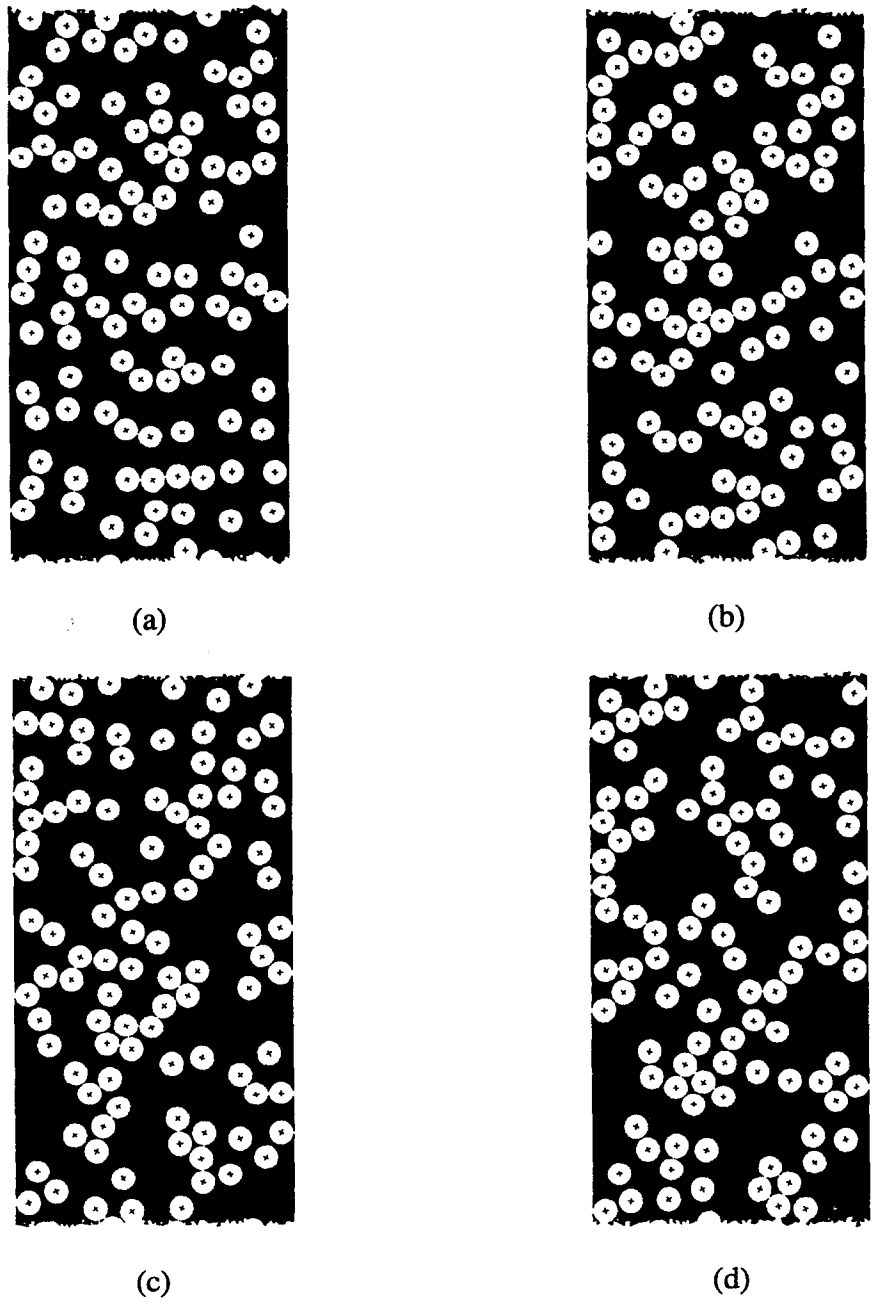

Figure 7. Down-flow with $W/d = 11$, $L/d = 22$, $\phi = 0.325$, $\rho_s/\rho_f = 1.1$, $\mathrm{Re} = 94.4$ and $\mathrm{d}\bar{p} = 0.336$. The figures show the snap shots of the flow field at four time instants, (a) $t^* = 5.29$, (b) $t^* = 8.31$, (c) $t^* = 10.9$ and (d) $t^* = 13.0$.

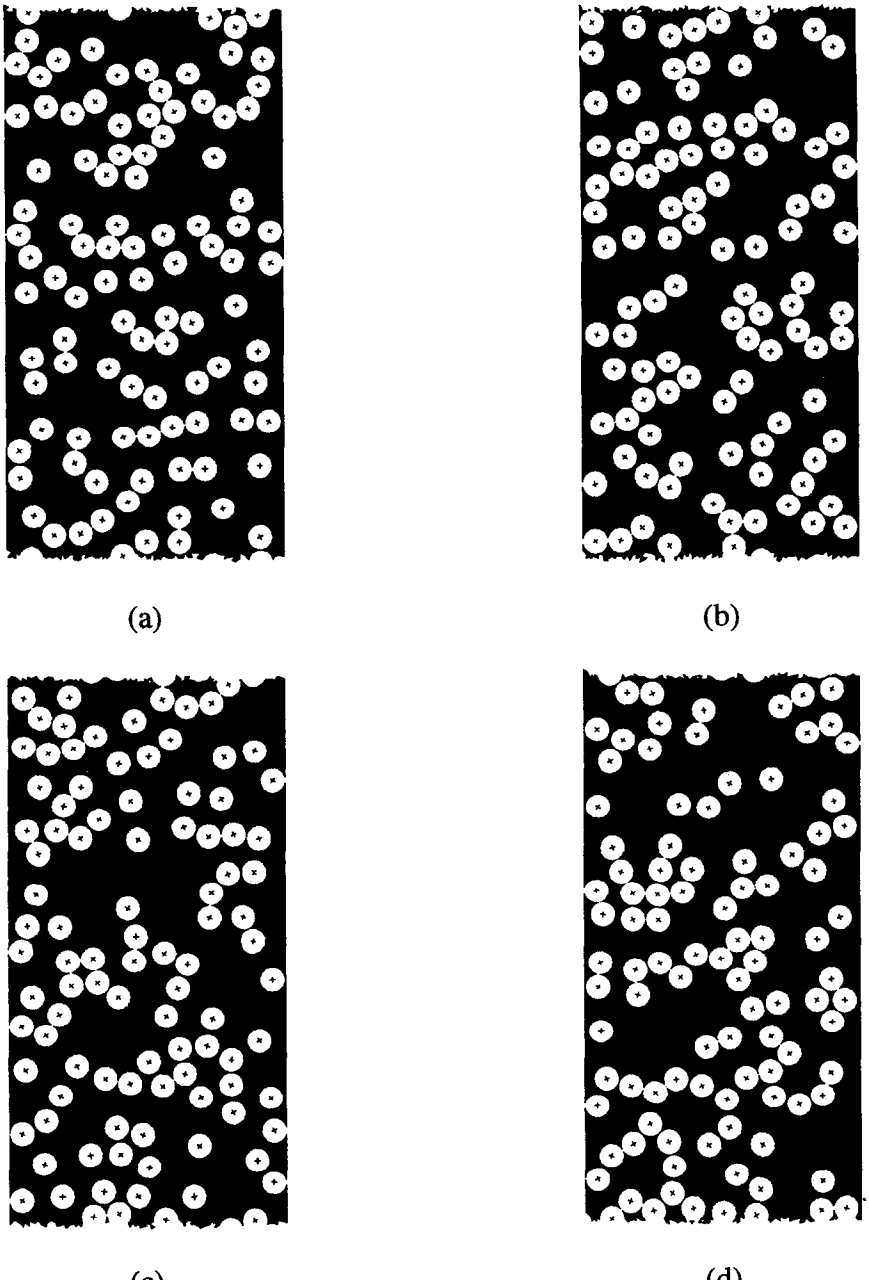

Figure 8. Upflow with $W/d = 11$, $L/d = 22$, $\phi = 0.325$, $\rho_s/\rho_f = 1.1$, Re = 94.4 and $d\bar{p} = 0.449$. The figures show the snap shots of the flow field at four time instants, (a) $t^* = 6.80$, (b) $t^* = 11.3$, (c) $t^* = 14.8$ and (d) $t^* = 18.2$.

(figure 6). Many cross-stream arrays are evident in the figures. For this flow, there is no clear liquid layer next to the channel walls, although most of the shear occurs at the near wall region. In the bulk of the channel the mixture flows upward almost uniformly. For the flow at high Reynolds numbers, the particles do get very close to each other or toward the channel walls, and the particles may collide.

We next reduce the particle concentration by simulating the flow in a larger channel. The parameters for the simulation are: $W/d = 16$, $L/d = 32$, $\phi = 0.153$, $\rho_s/\rho_f = 1.1$, Re = 94.4 and $d\bar{p} = 0.336$. The results are presented in figure 9. In this flow, the lubrication layer next to the channel walls is very clear, especially at later times. The flow in the bulk of the channel is again

uniform. The particles seem to cluster as they move along the flow. The waves of the solid fraction could be diagnosed by doing averaging and statistical analysis, which will be the topic of our next study.

The simulated result on the migration of the particles in Poiseuille flow agrees and extends the results of Feng *et al.* (1994b) where the migration of a single particle in Poiseuille flow was studied. The current numerical simulation also qualitatively agrees with experiment observations of spheres in circular tubes where it was found that spheres more dense than the fluid in an upflow (or spheres less dense in a downflow) migrate towards the tube axis, while spheres less dense than the fluid

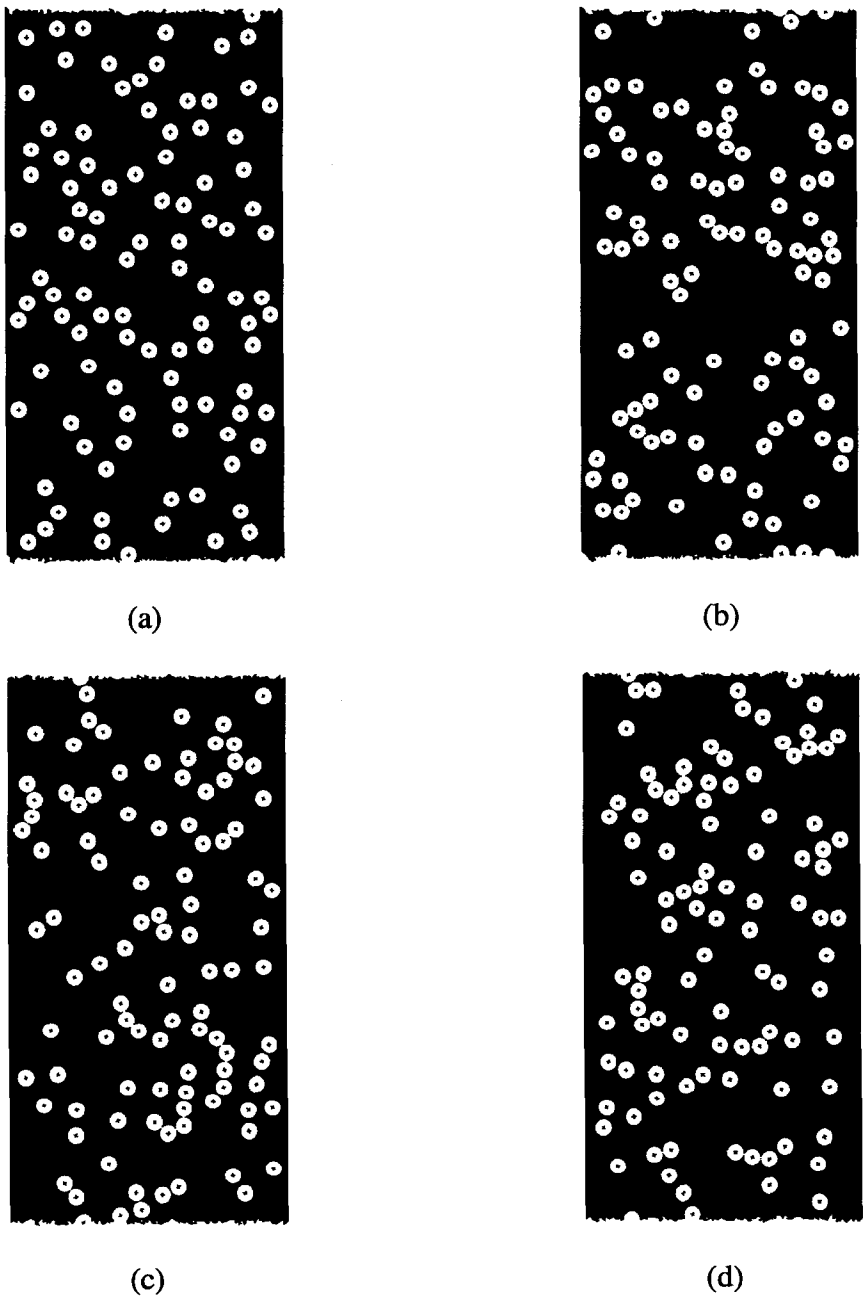

Figure 9. Upflow with $W/d = 16$, $L/d = 32$, $\phi = 0.153$, $\rho_s/\rho_f = 1.1$, Re = 94.4 and $d\bar{p} = 0.336$. The figures show the snap shots of the flow field at four time instants, (a) $t^* = 0$, (b) $t^* = 9.91$, (c) $t^* = 23.5$ and (d) $t^* = 34.0$.

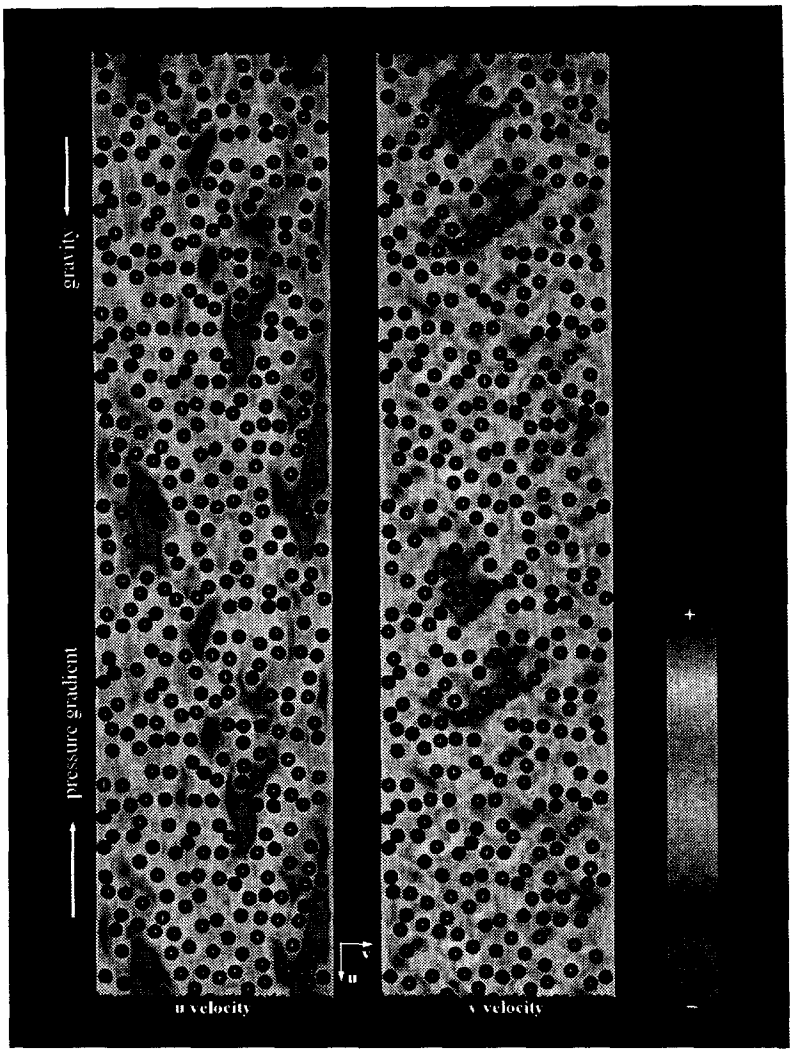

Figure 10. Four hundred particles flowing between a channel in two periodic cells. The solid–fluid mixture flows upwards against gravity. The flow parameters are $W/d = 16$, $L/d = 32$, $\phi = 0.306$, $\rho_s/\rho_f = 1.2$, $\mathrm{Re} = 12.7$ and $\mathrm{d}\bar{p} = 0.379$. The x component, u of the velocity is color coded on the elft and the y component, v, is on the right.

in an upflow (or spheres more dense in a downflow) migrate towards the tube wall [see, for example, Cox & Mason (1971), Brenner (1966) and Karnis *et al.* (1966)].

Finally, in figure 10 we demonstrate the capability of the code by presenting a snap shot of the simulation of 400 particles flowing between a channel in two periodic cells. In this simulation the total number of elements is around 30,000, the number of nodes in the mesh is around 60,000 and the total number of unknowns is about 170,000. The computation was performed on a four CPU CONVEX C240. It took about 15 min to advance one time step, in a vector mode using only one CPU. In this simulation, 600 time steps were performed.

7. CONCLUSIONS

We developed a numerical procedure based on an ALE Galerkin finite element technique to simulate the motion of a large number of solid particles in a flowing liquid. Using this procedure, we study the Poiseuille flow of solid–liquid mixtures in a vertical channel. The effects of the applied pressure gradient, the particle Reynolds number and the fraction of the solid loading on the flow pattern of the solid–liquid mixture are studied. It was found that when the applied pressure gradient is large enough to overcome the gravity (upflow), the particles migrate away from the channel walls and there is a clear liquid layer next to the walls which lubricates the flow. As the particle Reynolds

number is increased, particles interact more strongly and large clusters of particles are formed in the flow.

Acknowledgements—This work is supported by the National Science Foundation under an HPCC Grand Challenge Grant ECS-9527123 and CTS 94-10022 and by the Research Foundation of the University of Pennyslvania.

REFERENCES

Anderson, T. B. & Jackson, R. 1967 A fluid mechanical description of fluidized beds: equations of motion. *Ind. Engng Chem. Fundam.* **6,** 527–539.

Behr, M. & Tezduyar, T. E., 1994 Finite element solution strategies for large-scale flow simulations. *Comput. Methods Appl. Mech. Engng* **112,** 3–24.

Brady, J. F. 1993 Stockesian dynamics simulation of particulate flows. In *Particulate Two-phase Flow* (Edited by Roco, M. C.), pp. 971–998. Butterworth–Heinemann, New York.

Brady, J. F. & Bossis, G. 1988 Stokesian dynamics. *A. Rev. Fluid Mech.* **20,** 111–157.

Brenner, H. 1966 Hydrodynamic resistance of particles at small Reynolds numbers. *Adv. Chem. Engng* **6,** 287–439.

Cox, G. & Mason, S. G. 1971 Suspended particles in fluid flow through tubes. *A. Rev. Fluid Mech.* **3,** 291–316.

Drew, D. 1983 Mathematical modeling of two-phase flow. *A. Rev. Fluid Mech.* **15,** 261–291.

Esmaeeli, A. 1995 Numerical simulations of bubbly flows. Ph.D. thesis, University of Michigan. Advisor: G. Tryggvason.

Feng, J., Hu, H. H. & Joseph, D. D. 1994a Direct simulation of initial value problems for the motion of solid bodies in a Newtonian fluid. Part 1: sedimentation. *J. Fluid Mech.* **261,** 95–134.

Feng, J., Hu, H. H. & Joseph, D. D. 1994b Direct simulation of initial value problems for the motion of solid bodies in a Newtonian fluid. Part 2: Couette and Poiseuille flows. *J. Fluid Mech.* **277,** 271–301.

Feng, J., Huang, P. Y. & Joseph, D. D. 1995 Dynamic simulation of the motion of capsules in pipelines. *J. Fluid Mech.* **282,** 233–245.

George, P. L. 1991 *Automatic Mesh Generation, Application to Finite Element Methods.* Wiley, New York.

Hansbo, P. 1992 The characteristic streamline diffusion method for the time-dependent incompressible Navier–Stokes equations. *Comput. Meth. Appl. Mech. Engng* **99,** 171–186.

Hecht, F. & Saltel, E. 1990 Emc^2, a mesh editor for two dimensional contours. INRIA Report 118.

Helsa, T. I., Singh, P. & Joseph, D. D. 1996 The dynamical simulation of two-dimensional fluid/particle systems. In preparation.

Hu, H. H. 1996 "Motion of a circular cylinder in a viscous liquid between parallel plates". *Theor. Comput. Fluid Dynam.* In press.

Hu, H. H., Joseph, D. D. & Crochet, M. J. 1992 Direct simulation of fluid particle motions. *Theoret. Comput. Fluid Dynam.* **3,** 285–306.

Huang, P. Y., Feng, J. & Joseph, D. D. 1994 The turning couples on an elliptic particle settling in a vertical channel. *J. Fluid Mech.* **271,** 1–16.

Huerta, A. & Liu, W. K. 1988 Viscous flow with large free surface motion. *Comput. Meth. Appl. Mech. Engng* **69,** 277–324.

Hughes, T J. R., Franca L. P. & Mallet, M. 1987 A new finite element formulation for computational fluid dynamics: VI. Convergence analysis of the generalized SUPG formulation for linear time-dependent multi-dimensional advective–diffusive systems. *Comput. Meth. Appl. Mech. Engng* **63,** 97–112.

Hughes, T. J. R. & Hulbert, G. M. 1988 Space-time finite element methods for elasti-dynamics: formulations and error estimates. *Comput. Meth. Appl. Mech. Engng* **66,** 339–363.

Ishii, M. 1975 *Thermo-fluid Dynamic Theory of Two-phase Flows.* Eyrolles, Paris.

Johnson, A. & Tezduyar, T. E. 1994 Mesh update strategies in parallel finite element computations of flow with moving boundaries and interfaces. Research Report 94-018, Army High Performance Computing Research Center, University of Minnesota,

Johnson, A. & Tezduyar, T. E. 1995 Mesh generation and update strategies for parallel computation of 3D flow problems. Research Report 95-008, Army High Performance Computing Research Center, University of Minnesota.

Joseph, D. D. & Lundgren, T. S. 1990 Ensemble averaged and mixture theory equations for incompressible fluid particle suspensions. *Int. J. Multiphase Flow* **16,** 35–42.

Joseph, D. D. 1994, Interrogation of numerical simulation for modeling of flow induced microstructure. In *Liquid–Solid Flows* 1994, Vol. 189, pp. 31–40. American Society of Mechanical Engineers.

Karnis, A., Goldsmith, H. L. & Mason, S. G. 1966 The flow of suspensions through tubes, V. Inertial effects. *Can. J. Chem. Engng* **44,** 181–193.

Ladd, A. J. C. 1994 Numerical simulations of particulate suspensions via a discretized Boltzmann equation. *J. Fluid Mech.* **271,** 285–339.

Ladd, A. J. C., Colvin, M. E. & Frenkel, D. 1988 Applications of lattice-gas cellular automata to the Brownian motion of solids in suspension. *Phys. Rev. Lett.* **60,** 975–978.

Nomura T. & Hughes, T. J. R. 1992 An arbitrary Lagrangian–Eulerian finite element method for interaction of fluid and a rigid body. *Comput. Meth. Appl. Mech. Engng* **95,** 115–138.

Saad Y. & Schultz, M. 1986 GMRES: a generalized minimal residual algorithm for solving nonsymmetric linear systems. *SIAM J. Scient. Statist. Comput.* **7,** 856–869.

Sangani, A. S. & Didwania, A. K. 1993 Dynamic simulations of flows of bubbly liquids at large Reynolds numbers. *J. Fluid Mech.* **250,** 307–337.

Sangani, A. S. & Prosperetti, A. 1993 Numerical simulation of the motion of particles at large Reynolds numbers. In *Particulate Two-phase Flow* (Edited by Roco, M. C.), pp. 971–998. Butterworth–Heinemann, New York.

Smereka, P. 1993 On the motion of bubbles in a periodic box. *J. Fluid Mech.* **254,** 79–112.

Tezduyar, T. E., Liou, J. & Behr, M. 1992a A new strategy for finite element computations involving moving boundaries and interfaces—the DSD/ST procedure: I. The concept and the preliminary numerical tests. *Comput. Meth. Appl. Mech. Engng* **94,** 339–351.

Tezduyar, T. E., Liou, J., Behr, M. & Mittal, S. 1992b A new strategy for finite element computations involving moving boundaries and interfaces—the DSD/ST procedure: II. Computation of free-surface flows, two-liquid flows, and flows with drafting cylinders. *Comput. Meth. Appl. Mech. Engng* **94,** 353–371.

Unverdi, S. O. & Tryggvason, G. 1992 A front-tracking method for viscous, incompressible, multi-fluid flows. *J. Comput. Phys.* **100,** 25–37.

Zhang, D. Z., & Prosperetti, A. 1994 Averaged equations for inviscid disperse two-phase flow. *J. Fluid Mech.* **267,** 185–219.